



# Colloidal Mie Resonators for All-Dielectric Metaoptics

Sugimoto, Hiroshi  
Fujii, Minoru

---

(Citation)

Advanced Photonics Research, 2(4):2000111

(Issue Date)

2020-12-24

(Resource Type)

journal article

(Version)

Version of Record

(Rights)

© 2021 The Authors. Advanced Photonics Research published by Wiley-VCH GmbH.  
This is an open access article under the terms of the Creative Commons Attribution License, which permits use, distribution and reproduction in any medium, provided the original work is properly cited.

(URL)

<https://hdl.handle.net/20.500.14094/90009467>



# Colloidal Mie Resonators for All-Dielectric Metaoptics

Hiroshi Sugimoto\* and Minoru Fujii

High refractive index dielectric nanostructures exhibiting electric and magnetic Mie resonances offer a powerful platform for realizing unprecedented control of electromagnetic waves at the nanoscale and enhanced light–matter interactions. Dielectric metasurfaces with a variety of functionalities are realized due to the recent developments of nanofabrication technologies. In addition, colloidal dispersions of high refractive index dielectric nanoparticles have emerged as a special form of metamaterials that leads to a wider range of applications in photonics. This review focuses on the recent developments of colloidal Mie resonators made of moderate (2.5–3.5) to high (>3.5) refractive index dielectrics operating in the visible to near-infrared range. Starting from the brief summary of fundamental properties of spherical dielectric nanoparticles, fabrication methods of colloidal Mie resonators composed of different materials and optical functionalities such as the enhanced light–matter interactions, the chirality, and the structural color generation are overviewed.

## 1. Introduction

Optical responses of micro and nanoparticles have been attracting researchers for more than a century since Gustav Mie developed exact solutions of the Maxwell equations of an arbitrary size sphere under plane wave irradiation in 1908.<sup>[1]</sup> In 2012, Kuznetsov et al.<sup>[2]</sup> and Evlyukhin et al.<sup>[3]</sup> have rebooted the research fields by shedding light on magnetic resonances of a high refractive index dielectric nanosphere in the visible wavelength range. Unlike surface plasmon resonance of metal nanoparticles,<sup>[4]</sup> which consists mainly of electric multipolar modes,<sup>[5–10]</sup> high refractive index dielectric nanoparticles possess magnetic multipole modes as well as the electric ones. The presence of magnetic multipole resonance in the optical regime

allows us to design nanoantennas and metasurfaces that cannot be realized only by the electric resonances.<sup>[11–14]</sup> Another advantage of dielectric Mie resonators compared to the plasmonic counterparts is the low-loss feature in the optical regime. Ohmic losses and resultant heating in metal nanoparticles, which often limits their applications in biosensing and bioimaging,<sup>[15]</sup> can be avoided in dielectric Mie resonators.

The revival of dielectric Mie resonators for light manipulation owes a lot to recent advancements in nanofabrication technology such as electron beam lithography.<sup>[16–19]</sup> Complicated nanostructures have been produced with very high accuracy on a substrate and metasurfaces with a variety of functionalities have been developed.<sup>[20–24]</sup> In addition to nano-

antennas produced by nanofabrication technology, a colloidal dispersion of dielectric nanoparticles has been attracting attention as a new class of dielectric Mie resonators. As will be shown in this review, colloidal nanoparticles with controlled size and shape can be regarded as a “metafluid” with an unnaturally high or low refractive index. Nonfading structural coloration inks can be produced from colloidal nanoparticles. Furthermore, they can be a ubiquitous building block to produce nanoantennas and metasurfaces in large area.

In this review, we focus on colloidal dielectric Mie resonators having the resonance in the visible to near-IR range, and summarize the recent development. We first review the basic optical properties of a dielectric nanosphere based on Mie theory. We then overview material systems suitable for colloidal Mie resonators. We focus on moderate (2.5–3.5) to high refractive index (>3.5) materials. We then extend the discussion to hybrid systems composed of dielectric and metallic components. Finally, we show functionalities and applications of high refractive index colloidal nanoparticles.

## 2. Mie Resonance of a Spherical Nanoparticle

### 2.1. Mie Theory


According to Mie theory,<sup>[1,25]</sup> light scattering efficiency  $Q_{\text{sca}}$  of a spherical nanoparticle can be decomposed into a series of multipolar contributions, which is expressed as

$$Q_{\text{sca}} = \frac{2}{x^2} \sum_{n=1}^{\infty} (2n+1) (|a_n|^2 + |b_n|^2) \quad (1)$$

where  $x$  is a size parameter  $x = \pi d / \lambda$ ,  $\lambda$  is a wavelength,  $d$  is a diameter, and  $a_n$  and  $b_n$  are the Mie coefficients in terms of

Dr. H. Sugimoto, Prof. M. Fujii  
Department of Electrical and Electronic Engineering  
Graduate School of Engineering  
Kobe University  
Rokkodai, Nada, Kobe 657-8501, Japan  
E-mail: sugimoto@eedept.kobe-u.ac.jp

Dr. H. Sugimoto  
PRESTO  
JST  
Honcho 4-1-8, Kawaguchi, Saitama 332-0012, Japan

 The ORCID identification number(s) for the author(s) of this article can be found under <https://doi.org/10.1002/adpr.202000111>.

© 2021 The Authors. Advanced Photonics Research published by Wiley-VCH GmbH. This is an open access article under the terms of the Creative Commons Attribution License, which permits use, distribution and reproduction in any medium, provided the original work is properly cited.

DOI: 10.1002/adpr.202000111

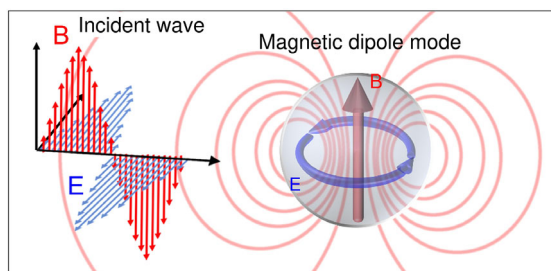


**Figure 1.** Schematic of the lowest order Mie resonance (MD mode). An electric field of incident light induces circular displacement current inside the particle, which results in the excitation of the MD mode.

spherical Bessel and Hankel functions. In general,  $a_n$  and  $b_n$  are referred to as electric-type (transverse magnetic) and magnetic-type (transverse electric) multipole modes. In a dielectric nanoparticle with a positive value of permittivity, the resonances are geometry-dependent and the condition for the lowest order resonance is satisfied when  $d \approx \lambda/n_i$ , where  $n_i$  is a refractive index of a nanoparticle.<sup>[16]</sup> **Figure 1** shows the schematic of a dielectric nanoparticle at the condition of the lowest

order resonance. In this condition, confined electric field forms a circular displacement current inside a nanoparticle, which induces a magnetic dipole (MD) resonance and enhanced magnetic field. This type of resonance is observed only in dielectric nanoparticles and is of particular interest in designing metaoptics.<sup>[14]</sup>

## 2.2. Effect of Refractive Index and Extinction Coefficient

A variety of high refractive index dielectric may be considered as a material for a Mie resonator. To achieve high-Q Mie resonance, both the refractive index ( $n_i$ ) and the extinction coefficient ( $\kappa_i$ ) are important. **Figure 2a** shows the scattering spectra calculated using Equation (1) for nonabsorbing ( $\kappa_i = 0$ ) dielectric spheres with different  $n_i$  from 2 to 5. The diameter of a sphere is changed depending on  $n_i$ ; the diameter is set to  $600/n_i$  nm, so that the MD resonance appears at the same wavelength range. Two distinct peaks assigned to electric dipole (ED) and MD modes are seen when  $n_i$  is larger than 3. The sphere with  $n_i < 3$  does not have clear peaks due to the low refractive index contrast to the surrounding environment ( $n = 1$ ), i.e., the low contrast lowers Q of the resonance. **Figure 2b** shows the scattering spectra of high refractive index ( $n = 4$ ) 150 nm diameter spheres with different

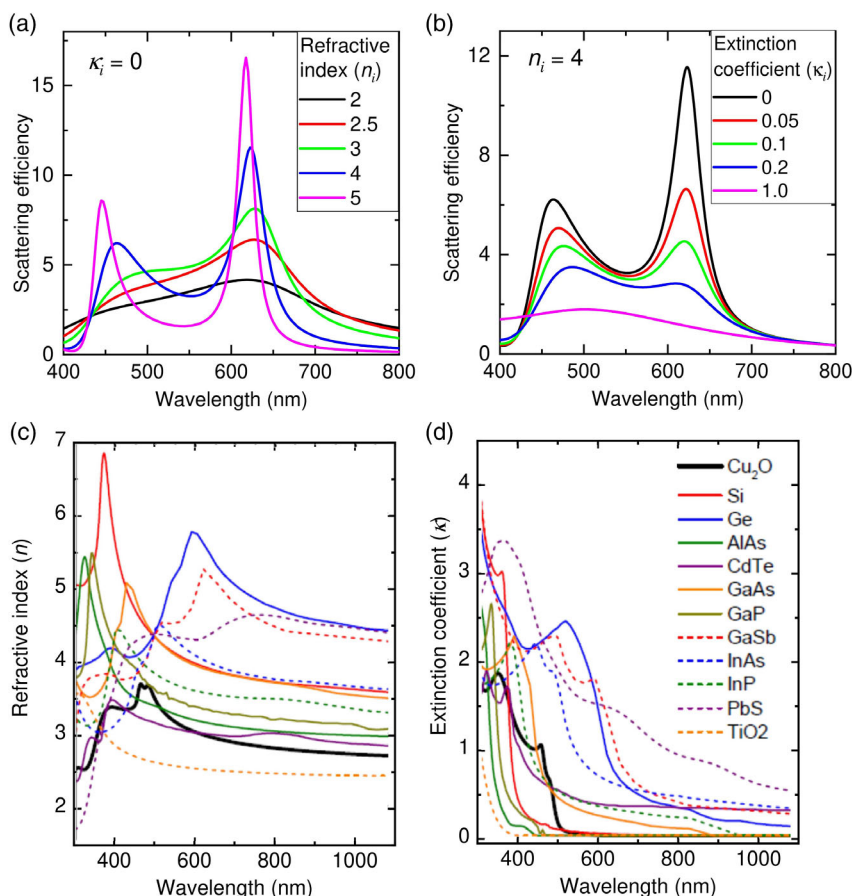


**Figure 2.** a) Scattering spectra of nonabsorbing spheres ( $d = 600/n_i$  nm) with different refractive indices ( $n_i$ ). b) Scattering spectra of high refractive index ( $n_i = 4$ ) spheres ( $d = 150$  nm) with different extinction coefficients. The surrounding medium is vacuum ( $n = 1$ ) and the contributions of ED and MD modes are considered. c) Refractive indices and d) extinction coefficients of dielectric materials. c,d) Reproduced with permission.<sup>[26]</sup> Copyright 2017, American Chemical Society.

extinction coefficients ( $\kappa_i$ ).  $\kappa_i$  strongly affects the spectral sharpness and the scattering efficiency; even  $\kappa_i$  as small as 0.1 almost halves the efficiency. From these results,  $n_i \gtrsim 3$  and  $\kappa_i \lesssim 0.1$  are desirable condition to have high-Q Mie resonance in a dielectric nanoparticle.

### 2.3. Material Exploration

Figure 2c,d shows refractive indices and extinction coefficients of high refractive index materials.<sup>[26]</sup> There are several materials with  $n_i \gtrsim 4$  in the visible range, for example, silicon (Si), lead sulfide (PbS), germanium (Ge), and indium arsenide (InAs). However, the extinction coefficients of PbS, Ge, and InAs in the visible range are too large ( $\kappa_i > 0.5$ ) to have high-Q resonance. In contrast, the extinction coefficient of Si is smaller than 0.1 above 440 nm and high-Q resonance is expected in almost the whole visible range. Therefore, Si is now one of the best candidates for all-dielectric metaoptics. In addition to high refractive index materials, moderate refractive index ( $n_i \approx 3$ ) materials are also used as Mie resonator nanoparticles because the synthesis routes are well established and high-quality colloidal nanoparticles are available. Furthermore, for some applications, high refractive index is not mandatory. Note that a moderate refractive index requires a larger diameter to obtain Mie resonances in the visible to near infrared (NIR) range.

## 3. Fabrications of Colloidal Mie Resonators

### 3.1. Silicon Nanoparticles

In this section, we summarize colloidal Mie resonators composed of high and moderate refractive index materials. The first one is crystalline Si. Among several high refractive index materials, crystalline Si has several advantages. The extinction coefficient is very small in the visible to near-IR range due to the indirect nature of the energy band structure. It is the most commonly used material in semiconductor industry and earth abundant. However, chemical synthesis of crystalline Si nanoparticles larger than 100 nm in diameter in solution is very difficult.<sup>[27]</sup> Therefore, the fabrication is based on either a top-down approach or a bottom-up growth in gas or in solid. Grown Si nanoparticles are afterward dispersed in a solution. A variety of growth processes of Si nanoparticles are summarized in a different review article.<sup>[27]</sup>

The first report on Mie resonance of colloidal Si nanoparticles was in 2012 by Shi et al.<sup>[28]</sup> However, the research was not on crystalline Si, but on amorphous hydrogenated Si (a-Si:H) prepared by chemical vapor deposition (CVD) using disilane ( $\text{Si}_2\text{H}_6$ ) as a precursor. Since a-Si has much higher  $\kappa$  ( $\approx 0.3$  at 600 nm) compared to crystalline Si ( $\approx 0.02$ ) in the visible range, its operation as a Mie resonator is limited to the near-IR range.<sup>[29]</sup> The scanning electron microscope (SEM) image of  $\text{Si}_{0.75}\text{H}_{0.25}$  colloids<sup>[30]</sup> in Figure 3a shows monodispersed particles with the size distribution of 2.2%. Postannealing reduces the porosity and the hydrogen content and the refractive index approaches that of crystalline Si.

A widely used method to fabricate Si nanoparticles is pulsed laser ablation of a Si wafer.<sup>[2,3]</sup> Laser ablation in a solution results

in the formation of colloidal Si nanoparticles.<sup>[31–33]</sup> A drawback of the process is the low controllability and uniformity of the size and shape of Si nanoparticles. Wakatsuki et al. demonstrated the formation of spherical Si nanoparticles from nonspherical ones in an aqueous solution using a nanosecond-pulsed laser melting method.<sup>[34]</sup> Laser ablation has also been used to directly transfer Si nanoparticles on a substrate. Zywiets et al.<sup>[35]</sup> developed a laser printing process, which allows a precise positioning of size-controlled Si nanoparticles on a substrate.

Verre et al.<sup>[36]</sup> developed a top-down approach for large-scale fabrication of silicon nanodisks using a hole-mask colloidal lithography (HCL) technique. The method enables production of nanoparticles from a whole 4 in. Si wafer. As schematically shown in Figure 3b, Si nanodisks are released from the substrate using hydrofluoric acids (HF) etching, resulting in a colloidal dispersion of Si nanodisks. The Si nanodisk colloids exhibit extinction peaks due to the Mie resonance from 550 to 1050 nm depending on the size. This method can be applied to produce different shape nanoparticles.<sup>[37]</sup> A standard deviation of the size distribution smaller than 3.5% is achieved by combining HCL and laser-induced transfer (LIT) technique.<sup>[38]</sup>

Chaabani et al. demonstrated that crystalline Si nanoparticles 100–200 nm in diameters can be produced by crashing Si lumps in water using a kitchen blender (Figure 3c), followed by size separation by centrifugation.<sup>[39]</sup> This method provides a facile, low-cost, and large-scale fabrication of crystalline Si Mie resonators. However, the size and shape distributions are inevitably large and the circularity of the particles is 81% (Figure 3d,e), which is smaller than those of typical colloidal metal nanoparticles ( $\approx 90\%$ ). The low uniformity of the size and the shape limits the tunability of the resonance wavelength.

A bottom-up process to produce almost perfectly spherical crystalline Si nanoparticles is recently developed.<sup>[40,41]</sup> Commercially available SiO lumps are annealed at temperatures higher than the melting point of Si (Figure 3f), which results in the formation of crystalline Si nanoparticles in a  $\text{SiO}_2$  matrix. Si nanoparticles are then liberated from a  $\text{SiO}_2$  matrix by HF etching. The SEM image in Figure 3g shows almost perfect spheres with the circularity factor of 97%.<sup>[41]</sup> Figure 3h shows the transmission electron microscope (TEM) image after size separation using a density gradient centrifugation process. The polydispersity decreases to 6%. The extinction peak of the Si nanoparticle colloids can be controlled from 440 to 800 nm by controlling the average diameter from 95 to 200 nm.

### 3.2. Nanoparticles of Moderate Refractive Index Materials

The process to grow moderate refractive index ( $n = 2.5\text{--}3.5$ ) nanoparticles is more mature than that to grow Si nanoparticles and very high-quality materials have been developed. Titanium dioxide ( $\text{TiO}_2$ ),<sup>[42,43]</sup> copper oxide ( $\text{Cu}_2\text{O}$ ),<sup>[44,45]</sup> Selenium (Se),<sup>[46,47]</sup> and boron (B)<sup>[48]</sup> have been proposed as moderate refractive index dielectrics. Figure 4a,b shows SEM images of submicrometer  $\text{TiO}_2$  nanoparticles synthesized *via* solvothermal nonaqueous technique.<sup>[42,43]</sup> High sphericity and small size distribution are achieved simultaneously. The extinction spectra agree relatively well with the calculated spectra. Another well-studied moderate refractive index material is  $\text{Cu}_2\text{O}$ .<sup>[44]</sup>



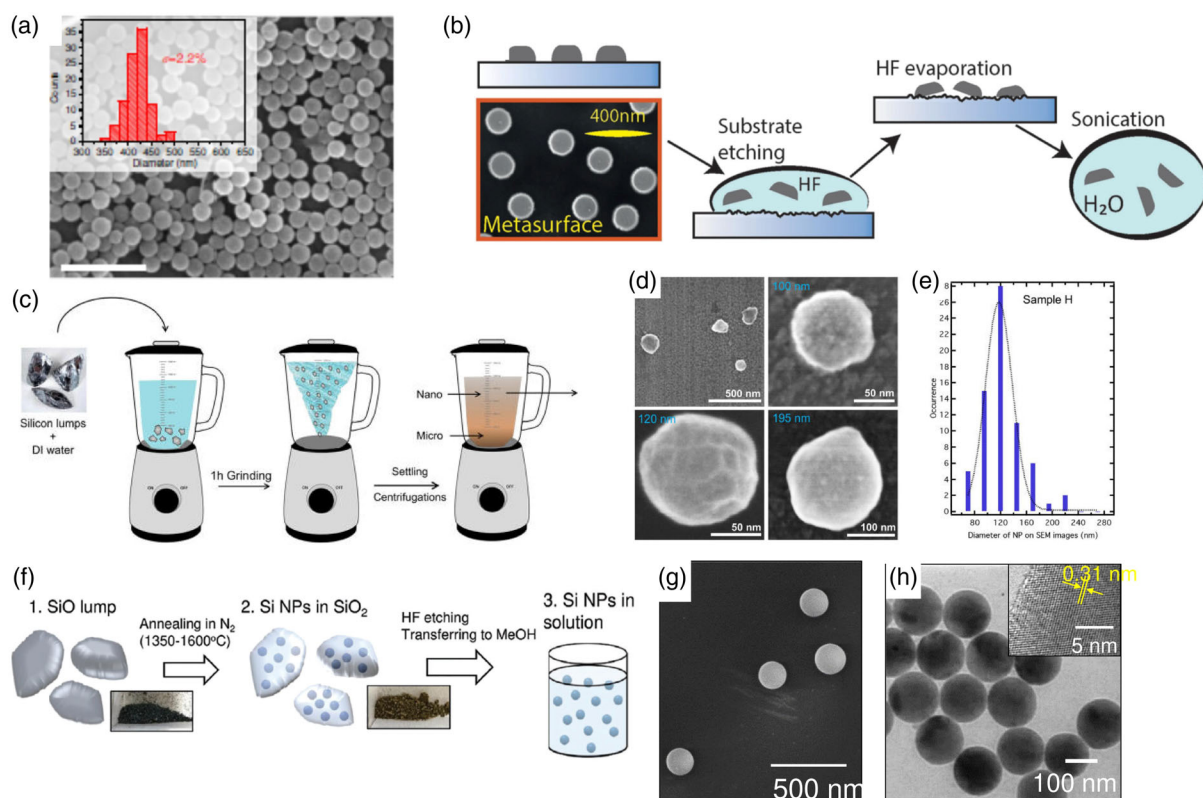


**Figure 3.** a) SEM image (scale bar 2000 nm) of  $\text{Si}_{0.75}\text{H}_{0.25}$  colloids. b) Schematic of the process to obtain Si nanodisk colloids from Si nanodisks on a substrate. c) Fabrication of Si nanoparticles using kitchen blender. d) SEM image and e) size distribution of nanoparticles prepared by the method in (c). f) Preparation of crystalline Si nanoparticles from SiO lumps. g) SEM and h) TEM images of Si nanoparticles prepared by the method in (f). a) Reproduced with permission.<sup>[30]</sup> Copyright 2013, Springer Nature. b) Reproduced with permission.<sup>[36]</sup> Copyright 2018, Wiley-VCH. c–e) Reproduced with permission.<sup>[39]</sup> Copyright 2019, American Chemical Society. f–h) Reproduced with permission.<sup>[41]</sup> Copyright 2020, Wiley-VCH.

$\text{Cu}_2\text{O}$  is a direct bandgap semiconductor with the bandgap of  $\approx 2.1$  eV and the refractive index is similar to those of chalcogenides. Wang and coworkers developed single-crystalline  $\text{Cu}_2\text{O}$  nanoparticles with uniform size and shape by a one-step wet-chemical method.<sup>[44,45]</sup> The average diameters are controlled from 126 to 340 nm and the size distributions are 6–9% (Figure 4c). The  $\text{Cu}_2\text{O}$  nanoparticles have Mie resonances in the visible region (Figure 4d). Different shape  $\text{Cu}_2\text{O}$  nanoparticles such as truncated octahedral<sup>[26]</sup> and cubes<sup>[49]</sup> are produced (Figure 4e). Se nanoparticles also attract much attention recently because polycrystalline Se exhibits transparency and moderate refractive index (2.8–3.2) in the visible range. Figure 4f shows highly uniform crystalline Se nanoparticles grown at a very low temperature (65 °C).<sup>[46,47]</sup>

#### 4. Optical Property of Single Nanoparticles

In dielectric nanoparticles, interference between the ED and MD modes provide a novel opportunity to tailor the far field scattering property. A well-known effect is the Kerker-type directionality,<sup>[50]</sup> which appears at the frequency that the ED and MD modes have the same amplitude; the destructive interference between the modes suppresses the backward scattering and enhances the

forward scattering.<sup>[50,51]</sup> Figure 5a shows calculated scattering spectrum of a 180 nm Si nanosphere.<sup>[52]</sup> Contributions from different modes are shown by different color curves. The yellow and green shaded regions indicate wavelength ranges in which ED and MD modes are in-phase and antiphase, respectively. At  $\approx 728$  nm where ED and MD overlap in-phase, the forward scattering is dominant (see left panel of Figure 5b), corresponding to the 1st Kerker condition. In contrast, at  $\approx 610$  nm, the backward scattering becomes dominant (see right panel of Figure 5b), which can be assigned to the 2nd Kerker condition.

Directional scattering of a single nanoparticle has been studied by microspectroscopy.<sup>[2,3,53–56]</sup> To avoid the effect of a substrate, a Si nanoparticle was placed on a very thin ( $\approx 8$  nm)  $\text{SiO}_2$  membrane and light scatterings to forward and backward directions were measured by dark-field optical microscope. The upper panel of Figure 5c shows the measured spectra, which agree very well with the calculated spectra for a Si nanosphere in free space shown in the lower panel of Figure 5c. The inset in Figure 5c is the TEM image of exactly the same Si nanosphere used for the scattering measurements.

The scattering spectrum of a Si nanoparticle is strongly modified when placed on a high refractive index dielectric or on a metal. Figure 6a shows scattering images of Si nanospheres placed on silica, Si, aluminum (Al), and gold (Au) substrates

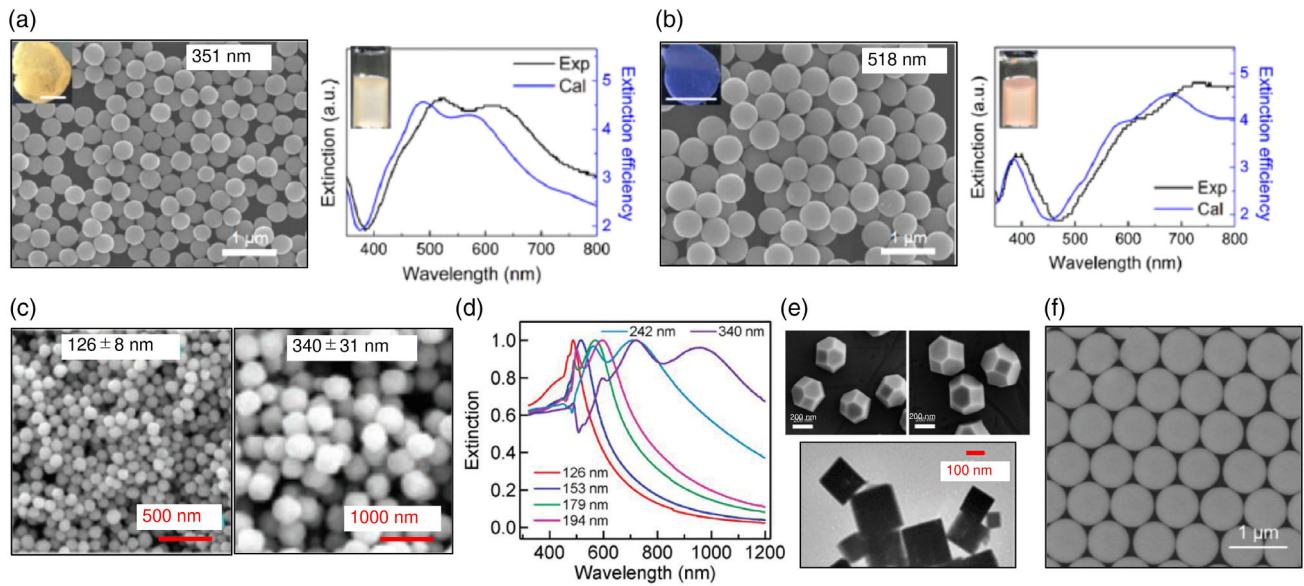


**Figure 4.** a,b) SEM images and extinction spectra of  $\text{TiO}_2$  nanoparticles with different diameters (351 and 518 nm). c) SEM images and d) extinction spectra of spherical  $\text{Cu}_2\text{O}$  nanoparticles. e) SEM and TEM images of  $\text{Cu}_2\text{O}$  nanoparticles with different shapes. f) SEM image of polycrystalline Se nanoparticles. a,b) Reproduced with permission.<sup>[43]</sup> Copyright 2019, American Chemical Society. c,d) Reproduced with permission.<sup>[45]</sup> Copyright 2020, Wiley-VCH. e) Reproduced with permission.<sup>[46]</sup> Copyright 2017, American Chemical Society; Reproduced with permission.<sup>[49]</sup> Copyright 2020, American Chemical Society. f) Reproduced with permission.<sup>[47]</sup> Copyright 2019, Wiley-VCH.

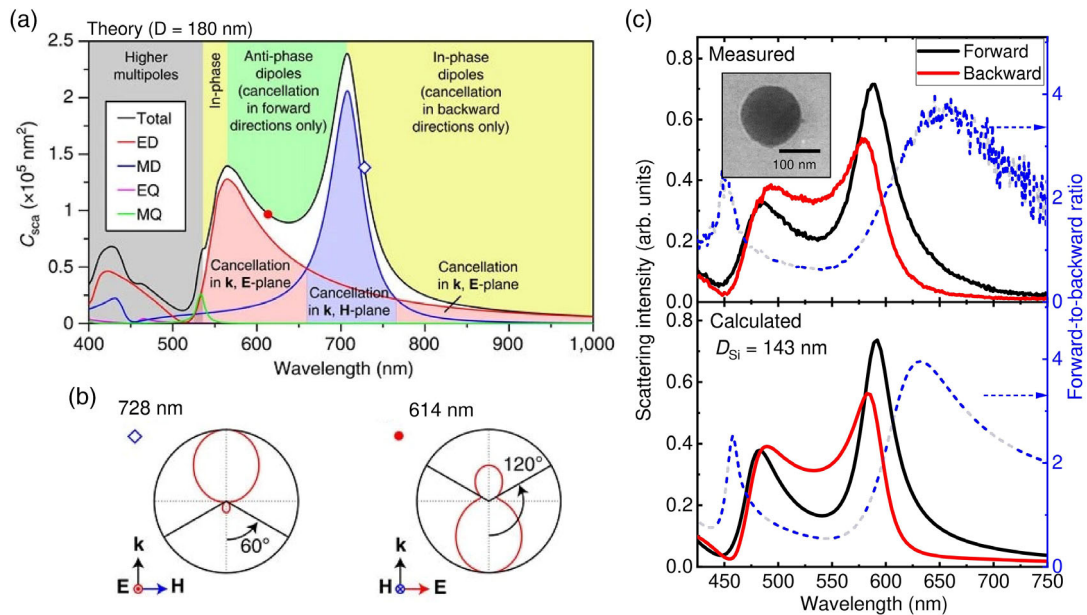


**Figure 5.** a) Total scattering cross section (black curve) and contributions of the ED (red curve), MD (blue curve), EQ (magenta curve), and MQ (green curve) of a Si sphere with the diameter of 180 nm. Shaded regions with different colors indicate the ranges in which ED and MD modes are in-phase (yellow) and antiphase (green). b) Far-field radiation patterns at 728 nm (left, blue hollow diamond) and at 614 nm (right, red solid circle) of the scattering spectrum in (a). c) Measured and calculated scattering spectra to forward (black curves) and backward directions (red curves) of a Si nanosphere (143 nm in diameter) shown in the inset. Blue dashed curves are the forward to backward ratios. a,b) Reproduced with permission.<sup>[52]</sup> Copyright 2016, Springer Nature. c) Reproduced with permission.<sup>[53]</sup> Copyright 2019, Wiley-VCH.

by drop-coating the colloidal solution on the substrates.<sup>[40]</sup> The average diameter of Si nanospheres is 120 nm. Near-field

coupling of a nanoparticle with a substrate significantly modifies the scattering color. Sinev et al.<sup>[57]</sup> assigned the effect to the

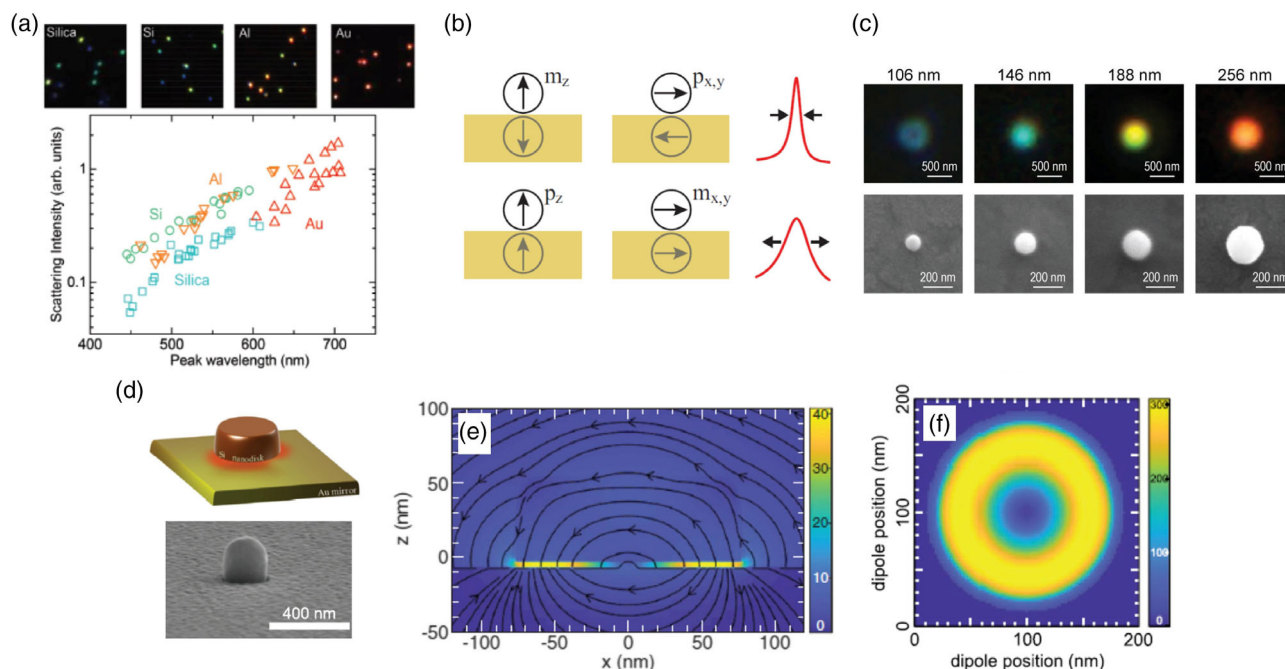


**Figure 6.** a) Scattering images of Si nanospheres on different substrates (silica, Si, Al, and Au) and the intensity of the strongest peak in the scattering spectra as a function of the wavelength for single Si nanospheres on different substrates. b) Schematic of coupling between ED ( $p_{x,y,z}$ ) and MD ( $m_{x,y,z}$ ) modes with image dipoles created in a metal substrate. c) Scattering and SEM images of size-controlled Cu<sub>2</sub>O nanoparticles placed on a Au film. d) Schematic illustration and SEM image, and e) electric field map of a Si nanodisk placed on a Au film. f) Map of Purcell enhancement (at 760 nm) of a z-oriented dipole placed at different positions. a) Reproduced with permission.<sup>[40]</sup> Copyright 2017, Wiley-VCH. b) Reproduced with permission.<sup>[57]</sup> Copyright 2016, Wiley-VCH. c) Reproduced with permission.<sup>[45]</sup> Copyright 2020, Wiley-VCH. d–f) Reproduced with permission.<sup>[60]</sup> Copyright 2020, Wiley-VCH.

coupling of the excited ED and MD with the image-dipoles (Figure 6b); depending on the dielectric functions of the substrates, the effect appears differently.<sup>[58]</sup> A particular interest is the in-phase coupling (Figure 6b,  $p_z$  and  $m_{x,y}$ ), which strongly enhances the scattering intensity.<sup>[59]</sup> Similar coupling effects appear in moderate refractive index nanoparticles such as Cu<sub>2</sub>O (Figure 6c).<sup>[45]</sup> The structure composed of a nanoparticle and a metal film can confine electromagnetic field into a very small gap, which enhances the light–matter interaction significantly.

In the case of a spherical nanoparticle on a metal film, the contact area is very small (point contact), which limits the effective size of a hot spot. In contrast, a nanodisk has a surface contact with a metal film and the hot spot is much larger. Maimaiti et al.<sup>[60]</sup> produced a colloidal solution of Si nanodisks by the method shown in Figure 3b and deposited it on metal surface to produce a nanodisk on a mirror structure (Figure 6d). In this configuration, the resonator can couple more efficiently to normal incident light (Figure 6e). The large scattering to absorption ratio of the Si nanodisk on a mirror system results in a large radiative Purcell factor. Figure 6f shows the Purcell enhancement map of a dipole placed in the gap region. Purcell enhancement reaches  $\approx 300$  for a dipole placed close to the edge of a nanodisk. This is an advantage of a hybrid system for light emission enhancement as will be discussed later.

## 5. Oligomers

Coupling between nanoparticles in dimers and oligomers provide additional functionalities such as field confinement in the gap,<sup>[61]</sup> directional scattering,<sup>[62–67]</sup> and chirality.<sup>[68]</sup> Several techniques have been developed to produce colloidal solutions of Mie resonator oligomers. Cho and coworkers<sup>[47]</sup> applied a colloidal self-assembly approach, i.e., capillary force-driven self-assembly, to a colloidal solution of polycrystalline Se nanoparticles, and succeeded in producing close-packed trimers. The scattering spectra in combination with the simulation revealed that electric and magnetic hot spots are formed at nanoparticle-to-nanoparticle interfaces (Figure 7a).

Oligomers composed of a Mie resonator and a plasmonic resonator are also an attractive system to manipulate light. Wang et al. proposed a heterodimer composed of a Si nanoparticle and a Au nanoparticle (Si–Au heterodimer) and demonstrated the efficient unidirectional scattering.<sup>[69]</sup> Our group developed a process to produce a colloidal solution of Si–Au heterodimers (Figure 7b).<sup>[53]</sup> The TEM image in Figure 7c shows a heterodimer composed of a 120 nm Si nanoparticle and a 100 nm Au nanoparticle. In this condition, the presence of a Au nanoparticle provides broad ED mode that overlaps with the MD mode of a Si nanoparticle. The overlap brings the Kerker-type forward scattering condition to the MD mode peak wavelength and enhances the forward directional scattering.<sup>[56,69]</sup>



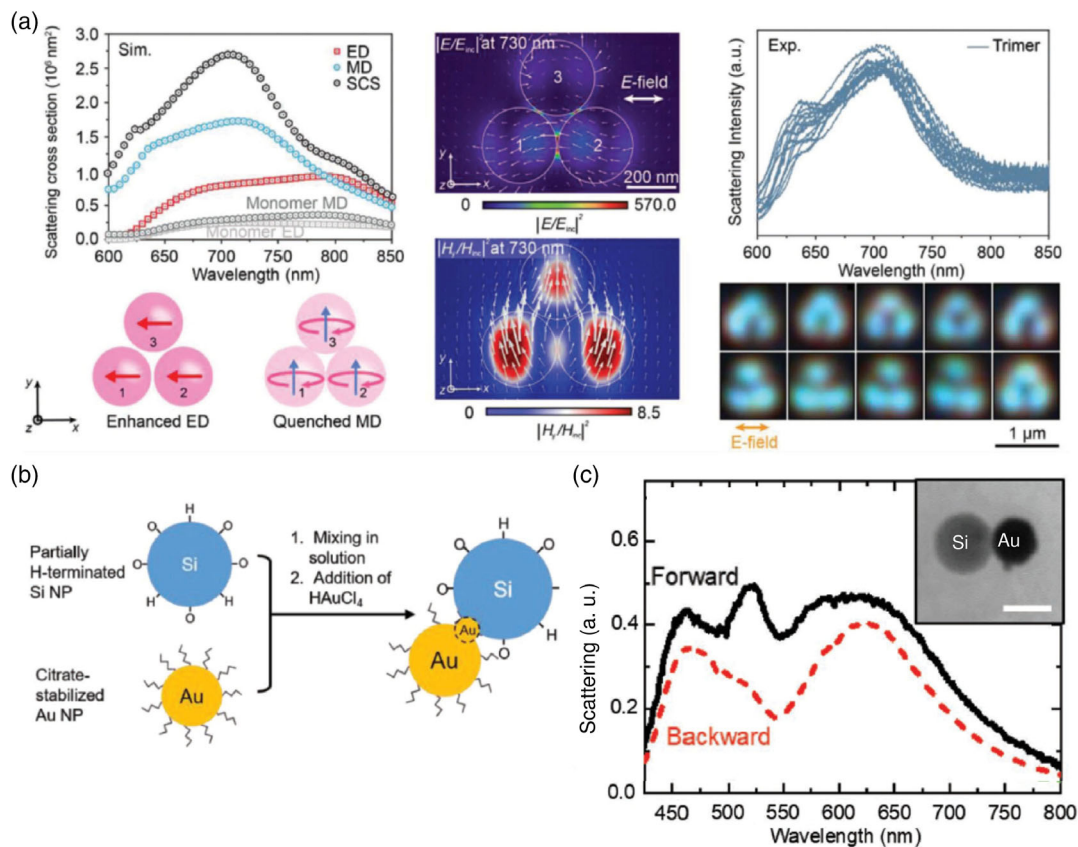


**Figure 7.** a) Se nanoparticle trimers composed of 300 nm diameter Se nanoparticles. Left, middle, and right panels correspond to calculated scattering cross sections, modal analysis of ED/MD resonances and electric/magnetic hot spots, measured bright-field scattering spectra, and microscope images, respectively. The incident light is polarized along the x-axis. b) Schematic illustration of Si-Au heterodimer formation process. c) Measured forward and backward scattering spectra of a Si-Au heterodimer shown in the inset. The scale bar is 100 nm. a) Reproduced with permission.<sup>[47]</sup> Copyright 2019, Wiley-VCH. b,c) Reproduced with permission.<sup>[53]</sup> Copyright 2019, Wiley-VCH.

## 6. Nanoparticle Assembly

Optical tweezers or optical manipulations have been applied to position nanoparticles on a substrate with high precision.<sup>[70–72]</sup>

**Figure 8a** shows schematic of the optical trapping of a nanoparticle under laser irradiation;  $F_r$  and  $F_g$  represent the radiation and gradient forces acting on the nanoparticle.<sup>[38]</sup> Although  $F_r$  is along the direction of light propagation,  $F_g$  is oriented toward the highest field intensity. When the condition of  $F_g > -F_r$  is satisfied, the nanoparticle is deposited on the substrate. Zaza et al.<sup>[33]</sup> developed a technology to selectively deposit specific size particles from a colloidal solution of polydisperse Si nanoparticles (Figure 8b). The size selection mechanism is based on the size dependence of the MD resonance wavelength. By tuning the excitation laser wavelengths to 405, 532, and 640 nm, Si nanoparticles with the radii of  $43 \pm 6$ ,  $59 \pm 9$ , and  $73 \pm 7$  nm, respectively, are deposited.

Although the optical trapping technique provides great controllability, the scalability and thus the application field is limited. More versatile assembling methods have been developed in plasmonic nanoparticles. One of the successful one is the template guided self-assemble approach (Figure 8c).<sup>[73,74]</sup>

A polymer template is fabricated by photolithography and defines locations for subsequent self-assembling of nanoparticles. By assembling colloidal nanoparticles into template patterns, nanoparticle oligomers and arrays are obtained on a substrate. This process may be applied to colloidal Mie resonators once the quality, i.e., colloidal stability, size uniformity, etc., catches up with that of Au and Ag colloids.

## 7. Functionalities of Colloidal Mie Resonators

### 7.1. Nanoantenna for Emission Enhancement

In this section, we discuss potential applications of dielectric Mie resonators, especially colloidal Mie resonators. The most remarkable feature of a resonant nanoparticle is its ability to confine electromagnetic field into the scale smaller than the wavelength.<sup>[75–78]</sup> When an emitter is placed near a nanoantenna, light emission is enhanced; the enhancement factor (EF) of photoluminescence (PL) is expressed as

$$EF = \frac{\gamma_{\text{ex}}^{\text{NP}} Q^{\text{NP}} \eta^{\text{NP}}}{\gamma_{\text{ex}}^{\text{ref}} Q^{\text{ref}} \eta^{\text{ref}}} \quad (2)$$



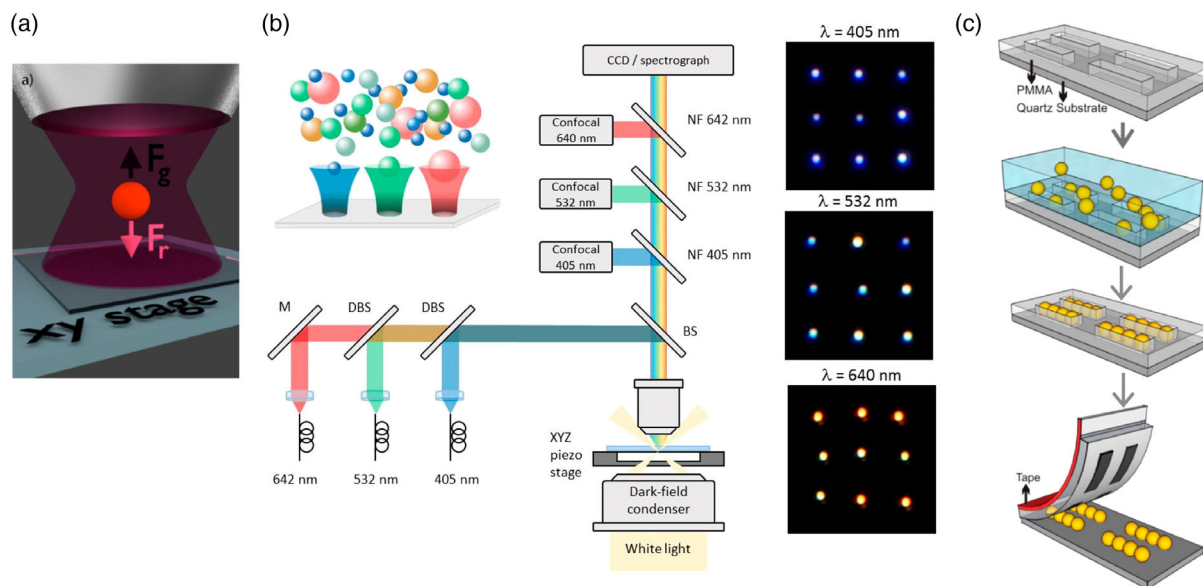


**Figure 8.** a) Schematic of optical trapping system. b) (Left) Schematic of experimental setup for size-selective optical printing process and (right) example grids of nanoparticles optically printed under 405, 532, and 640 nm light irradiation. c) Schematic of template-guided self-assembly process for plasmonic nanoparticles. a) Reproduced with permission.<sup>[38]</sup> Copyright 2019, American Chemical Society. b) Reproduced with permission.<sup>[33]</sup> Copyright 2019, American Chemical Society. c) Reproduced with permission.<sup>[73]</sup> Copyright 2013, American Chemical Society.

where  $\gamma_{\text{ex}}$  is an excitation rate of an emitter at the excitation wavelength,  $Q$  is a quantum efficiency, and  $\eta$  is an emission collection efficiency in the detection system. The superscripts “NP” and “ref” indicate the emitter with and without a nanoantenna, respectively.

In one photon-process,  $\gamma_{\text{ex}}$  depends on the electric field intensity ( $|E/E_0|^2$ ) modified by a nanoantenna. The excitation rate enhancement of an emitter by a Si nanoparticle is demonstrated by a simple system shown in **Figure 9a** in which a Si nanoparticle is placed on a thin layer of fluorescence dye.<sup>[40]</sup> The EF is proportional to the scattering intensity of a nanoparticle at the excitation wavelength, and it reaches  $\approx 200$ -fold when the resonance wavelength agrees with the excitation wavelength. The strong enhancement suggests that a Si nanoparticle nanoantenna does not require precise control of an emitter–antenna distance, which is indispensable in the metallic counterpart to avoid fluorescence quenching.

The strong field enhancement results in self-enhanced two (three) photon excited luminescence, the excitation rate of which is proportional to  $|E/E_0|^4$  ( $|E/E_0|^6$ ), from a Si nanoparticle.<sup>[79]</sup> Figure 9b shows the scattering and two-photon excited luminescence spectra of a Si nanoparticle 200 nm in diameter. The excitation wavelength (775 nm) is tuned to near the MD resonance, and the enhancement of the up-converted luminescence is observed at the magnetic quadrupole (MQ) and electric quadrupole (EQ) resonances. In this case, a Si nanoparticle acts as a cavity to confine excitation light and an antenna to efficiently couple the emission to far field propagation light.

In addition to the excitation efficiency, the quantum efficiency is enhanced *via* the enhancement of the local density of photonic states, which is characterized by the Purcell factor induced by a resonator.<sup>[80–82]</sup> However, the Purcell factor of a dielectric

nanoantenna is expected to be smaller than that of plasmonic nanoantennas due to the smaller field confinement. To simultaneously achieve a strong field confinement and a small nonradiative loss, a hybrid system composed of a dielectric nanoparticle placed on a metal mirror (NPoM) was proposed.<sup>[60,82,83]</sup> Yang<sup>[81]</sup> performed detailed comparison of the Q-factor, the mode volume, and the radiative Purcell factor between dielectric, dielectric–metal, and all-metal systems and demonstrated that a larger Purcell factor and a higher quantum efficiency can be simultaneously achieved in a dielectric NPoM. The large Purcell factor of a dielectric NPoM was experimentally verified by Maimaiti et al.<sup>[60]</sup> by means of cathodoluminescence mapping. The quantum efficiency enhancement is also experimentally demonstrated in a Si NPoM system formed by a solution-based process (Figure 9c).<sup>[83]</sup> A Si nanoparticle is placed on a Au mirror via a monolayer of Si quantum dots (QDs). A Si nanoparticle enhances the QD emission by sevenfold compared to that on a flat Au film. A rough estimation suggests that the enhancement reaches 700-fold at the hot spot. In this system, enhancements of the excitation rate and the collection efficiency are small, and thus, the quantum efficiency enhancement by the Purcell effect is the dominant enhancement mechanism. Later, Yang et al. experimentally demonstrated 42-fold decay rate enhancement in a similar structure, that is, a Si nanoparticle is placed on a Au film *via* a QD layer.<sup>[82]</sup> Another advantage of a dielectric NPoM compared to the plasmonic counterpart is the wider enhancement band due to the broader resonances.<sup>[83]</sup>

The Purcell enhancement of fluorescence occurs in the regime of weak coupling. To achieve strong coupling, an emitter with a large oscillator strength such as J-aggregates<sup>[84,85]</sup> and a transition metal dichalcogenide monolayer are studied.<sup>[86,87]</sup> Figure 9d shows the scattering spectra of a Cu<sub>2</sub>O nanoparticle

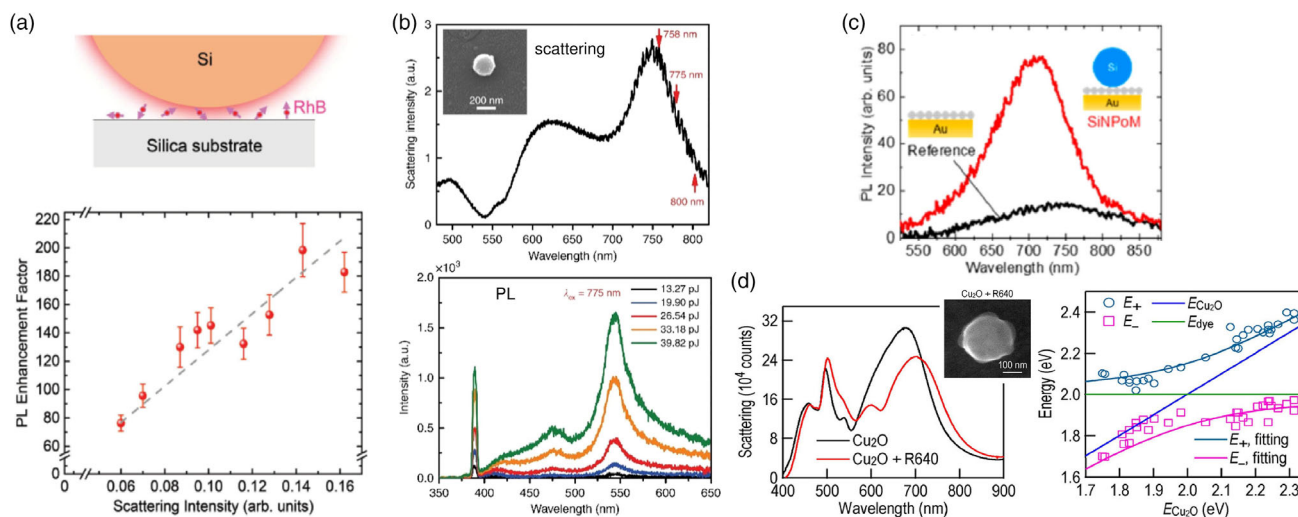


**Figure 9.** a) (Upper panel) Schematic of the structure to study fluorescence enhancement by a Si nanoparticle. A Si nanoparticle is placed on a dye-coated substrate. (Lower panel) PL EF as a function of scattering intensity at the excitation wavelength obtained for nine single Si nanospheres. b) Scattering spectrum and nonlinear emission spectrum excited at 775 nm for a 192 nm Si nanoparticle. c) PL spectra of a QD monolayer on a Au film without (black curve) and with a Si nanoparticle on top (red curve). d) (Left panel) Scattering spectra of single Cu<sub>2</sub>O nanoparticles before and after coating with R640 aggregates. (Right panel) Scattering peak energy of R640 aggregates-coated Cu<sub>2</sub>O nanoparticles as a function of the resonance energy of pristine Cu<sub>2</sub>O nanospheres.  $E^+$  and  $E^-$  are fitted with the formulas derived from the coupled harmonic oscillator model. a) Reproduced with permission.<sup>[40]</sup> Copyright 2017, Wiley-VCH. b) Reproduced with permission.<sup>[79]</sup> Copyright 2018, Springer Nature. c) Reproduced with permission.<sup>[83]</sup> Copyright 2018, American Chemical Society. d) Reproduced with permission.<sup>[85]</sup> Copyright 2018, American Chemical Society.

with and without rhodamine (R640) aggregates. The resonance coupling modifies the scattering spectrum of a Cu<sub>2</sub>O nanoparticle. In the right panel of Figure 9d, an anticrossing behavior with the mode splitting of 0.30 eV is observed. Although this is the largest splitting energy reported in a Si nanosphere–J-aggregate system,<sup>[84]</sup> it is still not in the regime of strong coupling. A new structure, e.g., a core–shell structure composed of a Mie resonator and a shell of a large oscillator strength active material is proposed to achieve strong coupling in Mie resonators. Lepeshov et al.<sup>[86]</sup> theoretically demonstrated that strong coupling is achieved in a Si nanoparticle covered by a tungsten sulfide (WS<sub>2</sub>) monolayer at the magnetic Mie resonance frequency.

## 7.2. Structural Color Inks

Dielectric Mie resonators efficiently scatter incoming light at the resonant wavelength, and exhibit scattering-induced structural color. A high-resolution color printing using Mie resonators has been achieved in a planar structure produced by electron beam lithography.<sup>[88–92]</sup> Because of the small size of an individual Mie resonator, ultrahigh resolution exceeding the optical diffraction limit can be achieved, although the device area is usually very small.

To achieve large area structural coloration by Mie resonators, Mie resonator color inks that are capable of being coated or inkjet printed on a substrate have been developed. Kim et al.<sup>[93]</sup> presented hollow carbon–silica nanospheres that exhibit angle-independent Mie scattering. The carbon inside the hollow silica increases the effective refractive index and the extinction

coefficient. The resonant wavelength is precisely tuned by the shell thickness. In this system, the color originates from the combination of the ED scattering and the absorption similar to the case of melanin nanoparticles.<sup>[94]</sup> In contrast, a high index Mie resonator such as a Si nanoparticle exhibits a vivid color due to the strong MD scattering. Figure 10a shows scattering images and spectra of single Si nanoparticles.<sup>[41]</sup> The scattering color is tunable in a wide range just by changing the diameters (see Figure 10b). By exploiting the scattering color of individual nanoparticles, our group developed structural color inks of almost monodispersed crystalline Si nanoparticles. Reduction of size distribution of Si nanoparticles to less than 10% results in solutions with vivid colors (Figure 10c). The backscattering spectra (diffuse reflectance spectra) in Figure 10d show the large tunability of the resonance wavelength covering the entire visible range by changing the size from 95 to 200 nm. Inks composed of a water solution of Si nanoparticles and a polymer binder can paint flexible substrate in  $\approx 1$  cm<sup>2</sup> range as shown in the photos in Figure 10e.

## 7.3. Functional Fluids and Solids

Colloidal dispersion of nanoparticles exhibiting optical magnetism is referred to as a “metafluid” which was first developed using plasmonic nanoparticle clusters (i.e., plasmonic molecules).<sup>[95–98]</sup> Metafluids possess unnaturally high or low effective refractive index and can be integrated into conventional optical components by solution-based processes.<sup>[95–98]</sup> Recently, Hinamoto et al.<sup>[99]</sup> demonstrated that a solution of size-purified Si nanospheres exhibits a strong optical magnetism (Figure 11a)

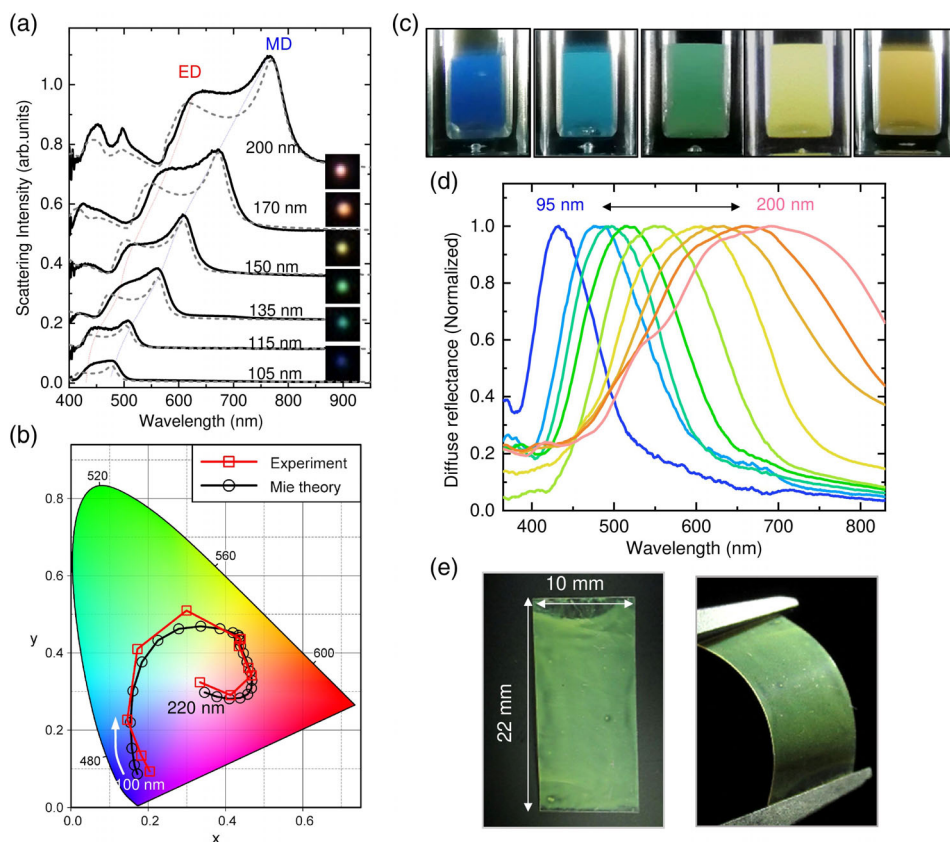


**Figure 10.** a) Scattering spectra of single Si nanoparticles with different diameters (105–200 nm) on glass substrate. Corresponding dark field images are shown. b) CIE1931 chromaticity diagram and experimental color space values obtained from scattering spectra of single Si nanoparticles of different diameters (100–220 nm). Data obtained from calculated scattering spectra are also shown. c) Photos and d) diffuse reflectance spectra of solutions of size-separated Si nanoparticles. e) Photographs of Si nanoparticle–polyvinyl pyrrolidone binder composite films on PET substrates. a–e) Reproduced with permission.<sup>[41]</sup> Copyright 2020, Wiley-VCH.

and proposed that the solution can be regarded as an all-dielectric “metafluid.” The intensities of the MD and ED scattering separately measured using angle- and polarization-resolved scattering spectroscopy were almost the same. The observed MD/ED intensity ratio is much higher than those reported for plasmonic metafluids in the visible range<sup>[95,100]</sup> and comparable to that in the near-IR range.<sup>[96]</sup> The possibility to achieve unnaturally high ( $>3$ ), low, and even near-zero ( $<1$ ) refractive index in the metafluid is discussed using the extended Maxwell–Garnett (EMG) theory.

Self-assembled crystals composed of Mie resonant nanoparticles such as amorphous Si<sup>[30]</sup> and Se<sup>[47]</sup> nanoparticles also exhibit optical magnetism. Figure 11b shows a face-centered-cubic (FCC) crystal of Se nanoparticles with the volume fraction of  $\approx 0.5$ . They demonstrated theoretically and experimentally that Se nanoparticle FCC crystal exhibits magneto–dielectric bandgaps.

Chirality is one of the important functions in photonics because it allows additional degree of freedom to control light–matter interactions through circular polarization. Verre et al.<sup>[37]</sup> developed a Si chiral colloidal solution in which right-handed or left-handed 3D Si nanocrescents are dispersed (Figure 11c). Figure 11d shows extinction and circular dichroism

(CD) spectra of a colloidal suspension of right-handed Si nanocrescents. The Si nanocrescents’ solution exhibits CD. The large CD signal around 640 nm agrees with the CD spectrum of Si nanocrescents on a substrate.<sup>[37]</sup>

## 8. Conclusion

We have presented a brief overview of experimental studies on colloidal Mie resonators. The technology to produce nanoparticles of high and moderate refractive index materials is developing quickly, and the capability to control the size and shape is catching up to those of colloidal plasmonic nanoparticles. We introduced some promising functionalities of colloidal Mie resonators such as the structural color generation and the fluorescence enhancement as a nanoantenna. The latter one is especially attractive in biophotonics because the low-loss nature minimizes the local-heating, which is unavoidable in plasmonic nanoantennas.<sup>[75]</sup> In addition to the fluorescence enhancement, Mie resonances can be designed to enhance intrinsically small light absorption of dielectric nanoparticles. This may open up the application toward photodetectors.<sup>[101]</sup> The optical magnetism of dielectric Mie resonators enhances



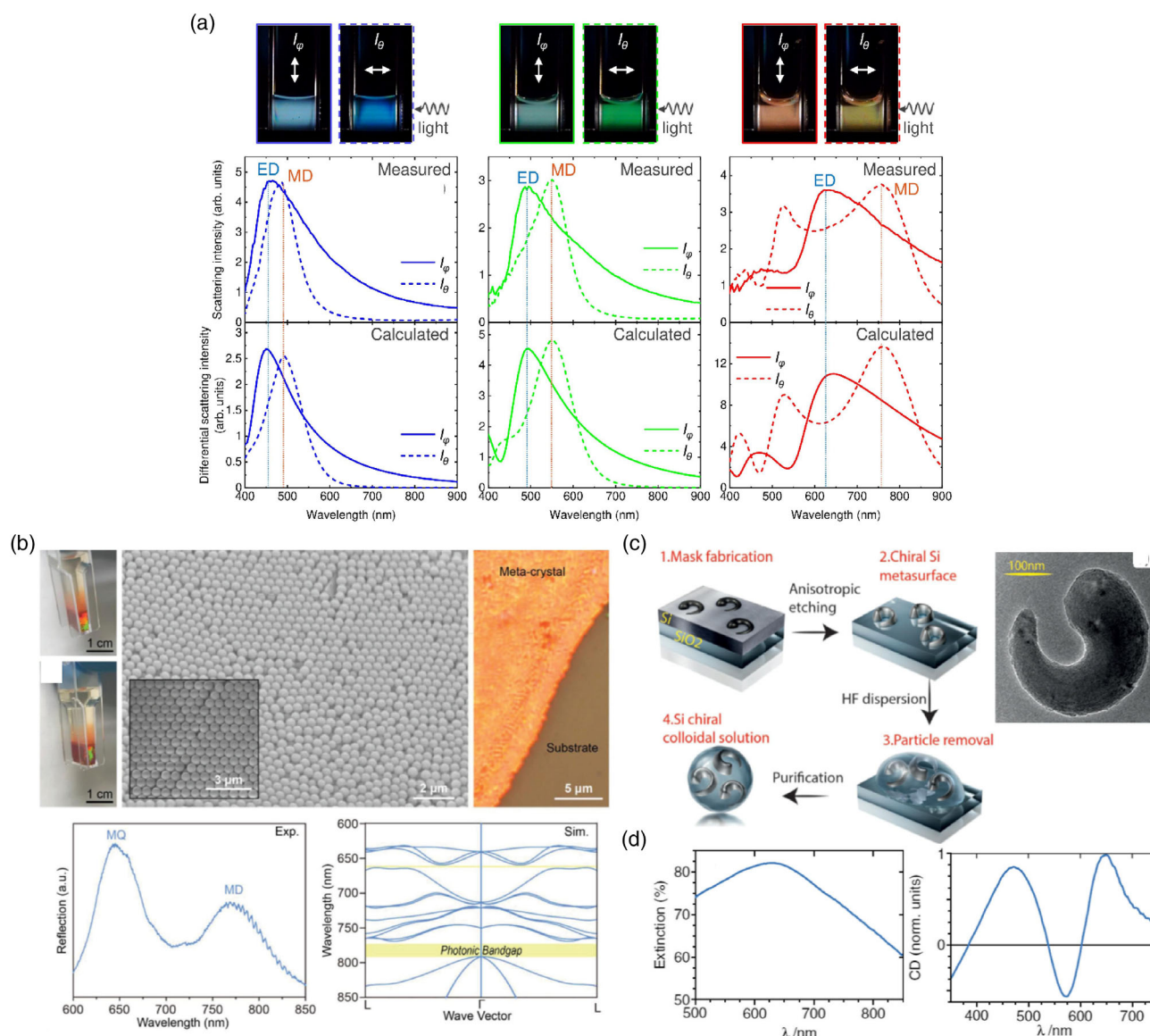


**Figure 11.** a) Photographs and scattering spectra measured by angle- and polarization-resolved spectroscopy of solutions of size-purified Si nanoparticles. Calculated spectra are also shown. b) (Upper panels) Photographs of 360 nm diameter Se colloids, and SEM and bright field microscope images of Se nanoparticle FCC crystal. (Lower panels) Measured reflection spectrum and simulated band diagram of self-assembled crystal of 360 nm diameter Se nanoparticles. Photonic bandgaps are observed around 660 and 785 nm. c) Fabrication process of colloidal 3D Si nanocrescents. d) Extinction and CD spectra of colloidal suspension of right-handed Si nanocrescents. a) Reproduced with permission.<sup>[99]</sup> Copyright 2020, American Chemical Society. b) Reproduced with permission.<sup>[47]</sup> Copyright 2018, Wiley-VCH. c,d) Reproduced with permission.<sup>[37]</sup> Copyright 2017, Wiley-VCH.

MD transitions of a molecule and an ion,<sup>[102]</sup> which paves the way to totally new photochemical reactions. Colloidal Mie resonators, including nanospheres, nanodisks, oligomers, Janus particles, chiral particles, etc., can also be a precursor to produce metasurfaces and solid-state photonic devices by a printing process. Development of technology to assemble these particles on a substrate with a high precision is crucial to produce a variety of metamaterials from colloidal Mie resonators.

## Acknowledgements

H.S. acknowledges the support provided by JST, PRESTO Grant number JPMJPR19T4. This work was partly supported by JSPS KAKENHI Grant number 18KK0141.

## Conflict of Interest

The authors declare no conflict of interest.



## Keywords

colloid, light manipulation, metamaterials, metasurfaces, Mie resonances, nanoantennas

Received: October 26, 2020

Revised: November 29, 2020

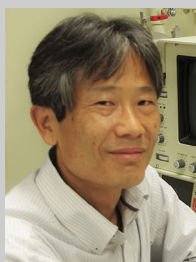
Published online: February 15, 2021

- [1] G. Mie, *Ann. Phys.* **1908**, 330, 377.
- [2] A. I. Kuznetsov, A. E. Miroshnichenko, Y. H. Fu, J. Zhang, B. Luk'yanchuk, *Sci. Rep.* **2012**, 2, 492.
- [3] A. B. Evlyukhin, S. M. Novikov, U. Zywietz, R. L. Eriksen, C. Reinhardt, S. I. Bozhevolnyi, B. N. Chichkov, *Nano Lett.* **2012**, 12, 3749.
- [4] V. Giannini, A. I. Fernández-Domínguez, S. C. Heck, S. A. Maier, *Chem. Rev.* **2011**, 111, 3888.
- [5] A. Campion, P. Kambhampati, *Chem. Soc. Rev.* **1998**, 27, 241.
- [6] W. E. Smith, *Chem. Soc. Rev.* **2008**, 37, 955.
- [7] G. M. Akselrod, C. Argyropoulos, T. B. Hoang, C. Ciraci, C. Fang, J. Huang, D. R. Smith, M. H. Mikkelsen, *Nat. Photonics* **2014**, 8, 835.
- [8] J. Dong, Z. Zhang, H. Zheng, M. Sun, *Nanophotonics* **2015**, 4, 472.
- [9] A. D. Boardman, A. V. Zayats, *Handb. Surf. Sci.* **2014**, 4, 329.
- [10] G. F. Walsh, L. Dal Negro, *Nano Lett.* **2013**, 13, 3111.
- [11] I. Staude, J. Schilling, *Nat. Photonics* **2017**, 11, 274.
- [12] S. Jahani, Z. Jacob, *Nat. Nanotechnol.* **2016**, 11, 23.
- [13] R. Paniagua-Domínguez, B. Luk'yanchuk, A. I. Kuznetsov, in *Dielectric Metamaterials* (Eds: I. Brener, S. Liu, I. Staude, J. Valentine, C. B. T.-D. M. Holloway), Elsevier, Amsterdam/New York **2020**, pp. 73–108.
- [14] S. Kruk, Y. Kivshar, *ACS Photonics* **2017**, 4, 2638.
- [15] G. Baffou, R. Quidant, *Laser Photonics Rev.* **2013**, 7, 171.
- [16] A. I. Kuznetsov, A. E. Miroshnichenko, M. L. Brongersma, Y. S. Kivshar, B. Luk'yanchuk, *Science* **2016**, 354, aag2472.
- [17] D. G. Baranov, D. A. Zuev, S. I. Lepeshov, O. V. Kotov, A. E. Krasnok, A. B. Evlyukhin, B. N. Chichkov, *Optica* **2017**, 4, 814.
- [18] W. Liu, Y. S. Kivshar, *Opt. Express* **2018**, 26, 13085.
- [19] M. Decker, I. Staude, M. Falkner, J. Dominguez, D. N. Neshev, I. Brener, T. Pertsch, Y. S. Kivshar, *Adv. Opt. Mater.* **2015**, 3, 813.
- [20] R. Paniagua-Domínguez, Y. F. Yu, E. Khaidarov, S. Choi, V. Leong, R. M. Bakker, X. Liang, Y. H. Fu, V. Valuckas, L. A. Krivitsky, A. I. Kuznetsov, *Nano Lett.* **2018**, 18, 2124.
- [21] C. Cui, C. Zhou, S. Yuan, X. Qiu, L. Zhu, Y. Wang, Y. Li, J. Song, Q. Huang, Y. Wang, C. Zeng, J. Xia, *ACS Photonics* **2018**, 5, 4074.
- [22] Z. Liu, Y. Xu, Y. Lin, J. Xiang, T. Feng, Q. Cao, J. Li, S. Lan, J. Liu, *Phys. Rev. Lett.* **2019**, 123, 253901.
- [23] A. Leitis, A. Tittl, M. Liu, B. H. Lee, M. B. Gu, Y. S. Kivshar, H. Altug, *Sci. Adv.* **2019**, 5, eaaw2871.
- [24] P. A. Jeong, M. D. Goldflam, S. Campione, J. L. Briscoe, P. P. Vabishchevich, J. Nogan, M. B. Sinclair, T. S. Luk, I. Brener, *ACS Photonics* **2020**, 7, 1699.
- [25] C. F. Bohren, D. R. Huffman, *Absorption and Scattering of Light by Small Particles*, John Wiley & Sons, New York **1983**.
- [26] M. D. Susman, A. Vaskevich, I. Rubinstein, *ACS Appl. Mater. Interfaces* **2017**, 9, 8177.
- [27] M. L. De Marco, S. Semlali, B. A. Korgel, P. Barois, G. L. Drisko, C. Aymonier, *Angew. Chem., Int. Ed.* **2018**, 57, 4478.
- [28] L. Shi, T. U. Tuzer, R. Fenollosa, F. Meseguer, *Adv. Mater.* **2012**, 24, 5934.
- [29] M. Wang, A. Krasnok, S. Lepeshov, G. Hu, T. Jiang, J. Fang, B. A. Korgel, A. Alù, Y. Zheng, *Nat. Commun.* **2020**, 11, 5055.
- [30] L. Shi, J. T. Harris, R. Fenollosa, I. Rodríguez, X. Lu, B. A. Korgel, F. Meseguer, *Nat. Commun.* **2013**, 4, 1904.
- [31] R. Intartaglia, K. Bagga, F. Brandi, *Opt. Express* **2014**, 22, 3117.
- [32] P. G. Kuzmin, G. A. Shafeev, V. V. Bukin, S. V. Garnov, C. Farcau, R. Carles, B. Warot-Frontrose, V. Guieu, G. Viau, *J. Phys. Chem. C* **2010**, 114, 15266.
- [33] C. Zaza, I. L. Violi, J. Gargiulo, G. Chiarelli, L. Schumacher, J. Jakobi, J. Olmos-Trigo, E. Cortes, M. König, S. Barcikowski, S. Schlücker, J. J. Sáenz, S. A. Maier, F. D. Stefani, *ACS Photonics* **2019**, 6, 815.
- [34] Y. Wakatsuki, Y. Ishikawa, N. Koshizaki, *Nanotechnology* **2020**, 31, 095601.
- [35] U. Zywietz, A. B. Evlyukhin, C. Reinhardt, B. N. Chichkov, *Nat. Commun.* **2014**, 5, 3402.
- [36] R. Verre, N. Odebo Länk, D. Andrén, H. Šípová, M. Käll, *Adv. Opt. Mater.* **2018**, 6, 1701253.
- [37] R. Verre, L. Shao, N. Odebo Länk, P. Karpinski, A. B. Yankovich, T. J. Antosiewicz, E. Olsson, M. Käll, *Adv. Mater.* **2017**, 29, 1701352.
- [38] V. Valuckas, R. Paniagua-Domínguez, A. Maimaiti, P. P. Patra, S. K. Wong, R. Verre, M. Käll, A. I. Kuznetsov, *ACS Photonics* **2019**, 6, 2141.
- [39] W. Chaabani, J. Proust, A. Movsesyan, J. Béal, A. L. Baudrion, P. M. Adam, A. Chehaidar, J. Plain, *ACS Nano* **2019**, 13, 4199.
- [40] H. Sugimoto, M. Fujii, *Adv. Opt. Mater.* **2017**, 5, 1700332.
- [41] H. Sugimoto, T. Okazaki, M. Fujii, *Adv. Opt. Mater.* **2020**, 8, 2000033.
- [42] Z.-Q. Li, W.-C. Chen, F.-L. Guo, L.-E. Mo, L.-H. Hu, S.-Y. Dai, *Sci. Rep.* **2015**, 5, 14178.
- [43] A.-M. Alam, K. Baek, J. Son, Y.-R. Pei, D. H. Kim, J.-H. Choy, J. K. Hyun, *ACS Appl. Mater. Interfaces* **2017**, 9, 23941.
- [44] S. Zhang, R. Jiang, Y.-M. Xie, Q. Ruan, B. Yang, J. Wang, H.-Q. Lin, *Adv. Mater.* **2015**, 27, 7432.
- [45] N. Li, H. Wang, Y. Lai, H. Chen, J. Wang, *Part. Part. Syst. Character.* **2020**, 37, 2000106.
- [46] Y. Cho, J.-H. Huh, K. J. Park, K. Kim, J. Lee, S. Lee, *Opt. Express* **2017**, 25, 13822.
- [47] Y. Cho, J. Huh, K. Kim, S. Lee, *Adv. Opt. Mater.* **2019**, 7, 1801167.
- [48] P. Liu, J. Yan, C. Ma, Z. Lin, G. Yang, *ACS Appl. Mater. Interfaces* **2016**, 8, 22468.
- [49] F. Mohammadparast, S. B. Ramakrishnan, N. Khatri, R. T. A. Tirumala, S. Tan, A. K. Kalkan, M. Andiappan, *ACS Appl. Nano Mater.* **2020**, 3, 6806.
- [50] M. Kerker, D.-S. Wang, C. L. Giles, *J. Opt. Soc. Am.* **1983**, 73, 765.
- [51] J. M. Geffrin, B. García-Cámara, R. Gómez-Medina, P. Albella, L. S. Froufe-Pérez, C. Eyraud, A. Litman, R. Vaillon, F. González, M. Nieto-Vesperinas, J. J. Sáenz, F. Moreno, *Nat. Commun.* **2012**, 3, 1171.
- [52] R. Paniagua-Domínguez, Y. F. Yu, A. E. Miroshnichenko, L. A. Krivitsky, Y. H. Fu, V. Valuckas, L. Gonzaga, Y. T. Toh, A. Y. S. Kay, B. Luk'yanchuk, A. I. Kuznetsov, *Nat. Commun.* **2016**, 7, 10362.
- [53] H. Sugimoto, T. Hinamoto, M. Fujii, *Adv. Opt. Mater.* **2019**, 7, 1900591.
- [54] Y. Tsuchimoto, T. Yano, T. Hayashi, M. Hara, *Opt. Express* **2016**, 24, 14451.
- [55] W. Wettling, J. Windscheif, *Solid State Commun.* **1984**, 50, 33.
- [56] Y. H. Fu, A. I. Kuznetsov, A. E. Miroshnichenko, Y. F. Yu, B. Luk'yanchuk, *Nat. Commun.* **2013**, 4, 1527.
- [57] I. Sinev, I. Iorsh, A. Bogdanov, D. Permyakov, F. Komissarenko, I. Mukhin, A. Samusev, V. Valuckas, A. I. Kuznetsov, B. S. Luk'yanchuk, A. E. Miroshnichenko, Y. S. Kivshar, *Laser Photon. Rev.* **2016**, 10, 799.
- [58] E. Xifré-Pérez, L. Shi, U. Tuzer, R. Fenollosa, F. Ramiro-Manzano, R. Quidant, F. Meseguer, *ACS Nano* **2013**, 7, 664.
- [59] Y. L. Kuo, S. Y. Chuang, S. Y. Chen, K. P. Chen, *ACS Omega* **2016**, 1, 613.
- [60] A. Maimaiti, P. P. Patra, S. Jones, T. J. Antosiewicz, R. Verre, *Adv. Opt. Mater.* **2020**, 8, 1901820.
- [61] R. M. Bakker, D. Permyakov, Y. F. Yu, D. Markovich, R. Paniagua-Domínguez, L. Gonzaga, A. Samusev, Y. Kivshar, B. Luk'yanchuk, A. I. Kuznetsov, *Nano Lett.* **2015**, 15, 2137.
- [62] J. H. Yan, P. Liu, Z. Y. Lin, H. Wang, H. J. Chen, C. X. Wang, G. W. Yang, *Nat. Commun.* **2015**, 6, 7042.

- [63] A. E. Miroshnichenko, Y. S. Kivshar, *Nano Lett* **2012**, 12, 17.
- [64] J. Yan, P. Liu, Z. Lin, H. Wang, H. Chen, C. Wang, G. Yang, *ACS Nano* **2015**, 9, 2968.
- [65] T. Shibanuma, T. Matsui, T. Roschuk, J. Wojcik, P. Mascher, P. Albella, S. A. Maier, *ACS Photonics* **2017**, 4, 489.
- [66] P. Albella, T. Shibanuma, S. A. Maier, *Sci. Rep.* **2016**, 5, 18322.
- [67] Y. Zhang, Y. Xu, S. Chen, H. Lu, K. Chen, Y. Cao, A. E. Miroshnichenko, M. Gu, X. Li, *ACS Appl. Mater. Interfaces* **2018**, 10, 16776.
- [68] X. Zhao, B. M. Reinhard, *ACS Photonics* **2019**, 6, 1981.
- [69] H. Wang, P. Liu, Y. Ke, Y. Su, L. Zhang, N. Xu, S. Deng, H. Chen, *ACS Nano* **2015**, 9, 436.
- [70] A. Andres-Arroyo, B. Gupta, F. Wang, J. J. Gooding, P. J. Reece, *Nano Lett.* **2016**, 16, 1903.
- [71] D. A. Shilkin, E. V. Lyubin, M. R. Shcherbakov, M. Lapine, A. A. Fedyanin, *ACS Photonics* **2017**, 4, 2312.
- [72] N. O. Länk, P. Johansson, M. Käll, *Opt. Express* **2018**, 26, 29074.
- [73] T. Chen, M. Pourmand, A. Feizpour, B. Cushman, B. M. Reinhard, *J. Phys. Chem. Lett.* **2013**, 4, 2147.
- [74] V. Flauraud, M. Mastrangeli, G. D. Bernasconi, J. Butet, D. T. L. Alexander, E. Shahrabi, O. J. F. Martin, J. Brugger, *Nat. Nanotechnol.* **2016**, 12, 73.
- [75] M. Caldarola, P. Albella, E. Cortés, M. Rahmani, T. Roschuk, G. Grinblat, R. F. Oulton, A. V. Bragas, S. A. Maier, *Nat. Commun.* **2015**, 6, 7915.
- [76] A. Krasnok, M. Caldarola, N. Bonod, A. Alú, *Adv. Opt. Mater.* **2018**, 6, 1701094.
- [77] S. Bidault, M. Mivelle, N. Bonod, *J. Appl. Phys.* **2019**, 126, 094104.
- [78] R. Regmi, J. Berthelot, P. M. Winkler, M. Mivelle, J. Proust, F. Bedu, I. Ozerov, T. Begou, J. Lumeau, H. Rigneault, M. F. García-Parajó, S. Bidault, J. Wenger, N. Bonod, *Nano Lett.* **2016**, 16, 5143.
- [79] C. Zhang, Y. Xu, J. Liu, J. Li, J. Xiang, H. Li, J. Li, Q. Dai, S. Lan, A. E. Miroshnichenko, *Nat. Commun.* **2018**, 9, 2964.
- [80] L. Novotny, B. Hecht, *Principles of Nano-Optics*, Cambridge University Press, Cambridge **2006**.
- [81] Y. Yang, O. D. Miller, T. Christensen, J. D. Joannopoulos, M. Soljačić, *Nano Lett.* **2017**, 17, 3238.
- [82] G. Yang, Y. Niu, H. Wei, B. Bai, H. B. Sun, *Nanophotonics* **2019**, 8, 2313.
- [83] H. Sugimoto, M. Fujii, *ACS Photonics* **2018**, 5, 1986.
- [84] H. Wang, Y. Ke, N. Xu, R. Zhan, Z. Zheng, J. Wen, J. Yan, P. Liu, J. Chen, J. She, Y. Zhang, F. Liu, H. Chen, S. Deng, *Nano Lett.* **2016**, 16, 6886.
- [85] Q. Ruan, N. Li, H. Yin, X. Cui, J. Wang, H. Q. Lin, *ACS Photonics* **2018**, 5, 3838.
- [86] S. Lepeshov, M. Wang, A. Krasnok, O. Kotov, T. Zhang, H. Liu, T. Jiang, B. Korgel, M. Terrones, Y. Zheng, A. Alú, *ACS Appl. Mater. Interfaces* **2018**, 10, 16690.
- [87] H. Wang, J. Wen, W. Wang, N. Xu, P. Liu, J. Yan, H. Chen, S. Deng, *ACS Nano* **2019**, 13, 1739.
- [88] Y. Nagasaki, M. Suzuki, J. Takahara, *Nano Lett.* **2017**, 17, 7500.
- [89] V. Flauraud, M. Reyes, R. Paniagua-Domínguez, A. I. Kuznetsov, J. Brugger, *ACS Photonics* **2017**, 4, 1913.
- [90] Z. Dong, J. Ho, Y. F. Yu, Y. H. Fu, R. Paniagua-Domínguez, S. Wang, A. I. Kuznetsov, J. K. W. Yang, *Nano Lett.* **2017**, 17, 7620.
- [91] V. Vashistha, G. Vaidya, R. S. Hegde, A. E. Serebryannikov, N. Bonod, M. Krawczyk, *ACS Photonics* **2017**, 4, 1076.
- [92] S. Sun, Z. Zhou, C. Zhang, Y. Gao, Z. Duan, S. Xiao, Q. Song, *ACS Nano* **2017**, 11, 4445.
- [93] S. Kim, V. Hwang, S. G. Lee, J. Ha, V. N. Manoharan, G. Yi, *Small* **2019**, 15, 1900931.
- [94] S. Cho, T. S. Shim, J. H. Kim, D.-H. Kim, S.-H. Kim, *Adv. Mater.* **2017**, 29, 1700256.
- [95] S. N. Shekholeslami, H. Alaeian, A. L. Koh, J. A. Dionne, *Nano Lett.* **2013**, 13, 4137.
- [96] Z. Qian, S. P. Hastings, C. Li, B. Edward, C. K. McGinn, N. Engheta, Z. Fakhraei, S.-J. Park, *ACS Nano* **2015**, 9, 1263.
- [97] K. Kim, S. Yoo, J.-H. Huh, Q.-H. Park, S. Lee, *ACS Photonics* **2017**, 4, 2298.
- [98] P. Wang, J. Huh, J. Lee, K. Kim, K. J. Park, S. Lee, Y. Ke, *Adv. Mater.* **2019**, 31, 1901364.
- [99] T. Hinamoto, S. Hotta, H. Sugimoto, M. Fujii, *Nano Lett.* **2020**, 20, 7737.
- [100] A. Alú, A. Salandrino, N. Engheta, *Opt. Express* **2006**, 14, 1557.
- [101] M. Garín, R. Fenollosa, R. Alcubilla, L. Shi, L. F. Marsal, F. Meseguer, *Nat. Commun.* **2014**, 5, 3440.
- [102] A. Vaskin, S. Mashhadi, M. Steinert, K. E. Chong, D. Keene, S. Nanz, A. Abass, E. Rusak, D.-Y. Choi, I. Fernandez-Corbaton, T. Pertsch, C. Rockstuhl, M. A. Noginov, Y. S. Kivshar, D. N. Neshev, N. Noginova, I. Staude, *Nano Lett.* **2019**, 19, 1015.



**Hiroshi Sugimoto** is an assistant professor at the Graduate School of Engineering, Kobe University, Japan. He received his Ph.D. in 2016 from Kobe University. From 2014 to 2015, he was also a visiting scientist at the Photonics Center at Boston University. After a short-term postdoctoral fellowship in Professor Fujii's group, he obtained his current position at Kobe University. His current research focuses on the development of novel dielectric and plasmonic nanomaterials for photonics and biophotonics applications.



**Minoru Fujii** received his doctorate degree from Kobe University in 1992 and then started working at Panasonic Corporation. He joined Kobe University in 1995. Since 2009, he has been a professor in the Graduate School of Engineering, Kobe University. From 2001 to 2002, he was a visiting scientist in the Technical University of Munich under the fellowship of the Alexander von Humboldt Foundation. His research interests include nanostructured semiconductor and metal materials for photonic and electronic applications.